

# Distribution characteristics of summer precipitation raindrop spectrum in Qinghai–Tibet Plateau

Fuzeng Wang<sup>1,2</sup>, Yao Huo<sup>1</sup>, Yaxi Cao<sup>1</sup>, Qiusong Wang<sup>1</sup>, Tong Zhang<sup>2</sup>, Junqing Liu<sup>3</sup>,  
Guangmin Cao<sup>4</sup>

<sup>1</sup>College of Electronic Engineering, Chengdu University of Information Technology, Chengdu 610225,  
China

<sup>2</sup>Key Laboratory of Land Surface Process and Climate Change in Cold and Arid Regions, Chinese  
Academy of Sciences, Lanzhou 730000, China

<sup>3</sup>Weather Modification Center for Tibet, Lhasa 850000, China

<sup>4</sup>Heilongjiang Meteorological Data center, Harbin 150000, China

*Correspondence to:* Guangmin Cao(ccgm909@163.com)

**Abstract:** To enhance the precision of precipitation forecasting in the Qinghai–Tibet Plateau region, a comprehensive study of both macro– and micro–characteristics of local precipitation is imperative. In this study, we investigated the particle size distribution, droplet velocity, droplet number density,  $Z$  (Radar reflectivity) –  $I$  (Rainfall intensity) relationship, and Gamma distribution of precipitation droplet spectra with a single precipitation duration of at least 20 minutes and precipitation of 5 mm or more at four stations (Nyalam, Lhasa, Shigatse, and Naqu) in Tibet during the recent years from June to August. The results are as follows: (1) In the fitting relationship curve between precipitation raindrop spectral particle size and falling speed at the four stations in Tibet, when the particle size was less than 1.5 mm, the four lines essentially coincided. When the particle size exceeded 1.5 mm, the speed in Nyalam was the highest, followed by Naqu, and the speed in Lhasa was the lowest. The falling speed of particles correlated with altitude. (2) The six microphysical characteristics at the four stations have different correlation relationships with altitude under different rainfall intensities.  $D_m$  exhibits a negative correlation with altitude at the same rainfall intensity; in contrast,  $D_v$  shows a positive correlation with altitude. For microphysical parameters such as  $D_d$  and  $D_p$ , a rainfall intensity of  $10 \text{ mm}\cdot\text{h}^{-1}$  serves as the boundary line, and they have different correlation relationships with altitude under the same rainfall intensity level. (3) The  $Z$ – $I$  relationships at the four stations exhibited variations. Owing to the proximity in altitude between Lhasa and Shigatse, as well as between Nyalam and Nagqu, the coefficients  $a$  and index  $b$  in the  $Z$ – $I$  relationships of the two groups of sites were relatively similar. (4) The fitting curves

30 of the Exponential and Gamma distributions of the precipitation particle size at the aforementioned four  
31 stations are largely comparable. The Exponential distribution fitting exhibits a slightly better effect. The  
32 parameter  $\mu$  in Gamma distribution decreases with the increase of altitude, while  $N_0$  and  $\lambda$  in Exponential  
33 distribution show a clear upward trend with altitude.

## 34 **1. Introduction**

35 The microphysical processes of cloud and precipitation over the Qinghai–Tibet Plateau significantly  
36 differ from those in low–altitude regions due to the high average altitude and complex, changeable terrain,  
37 resulting in a strong ground heating effect. Due to the terrain's influence, the plateau area has a limited  
38 number of observation stations, leading to a scarcity of precipitation records. Based on three atmospheric  
39 scientific experiments conducted over the Qinghai–Tibet Plateau, convective clouds exhibit high activity,  
40 although the precipitation intensity is moderate(Li et al., 2014; Jiang et al., 2002; Xu et al., 2006; Li et  
41 al., 2001). In the central part of the Plateau, convective clouds constitute 4% to 21%, with cumulonimbus  
42 clouds representing 21%. Additionally, the frequency of severe weather, such as thunderstorms and hail,  
43 surpasses that in other regions. In the majority of Qinghai–Tibet Plateau areas, convective cloud  
44 precipitation constitutes over 90% of the total (Chang and Guo, 2016). Particularly during the rainy  
45 season, convective processes are frequent with smaller horizontal scales, weaker intensities, and shorter  
46 durations. Due to observational constraints, short–term tests and satellite data (e.g., TRMM, CloudSat,  
47 and Aqua) are employed to investigate Tibetan Plateau precipitation, with a focus on liquid precipitation  
48 characteristics, including seasonal and diurnal variations and convective activity's liquid drop spectrum  
49 inversion(Ruan et al., 2015; Liu et al., 2015; Xiong et al., 2019; Zhang et al., 2018). The scarcity of  
50 observational data on cloud precipitation's physical processes in the Qinghai–Tibet Plateau results in  
51 limited studies on microscopic parameters' characteristics. The recent installation of a laser raindrop  
52 spectrometer enables a comprehensive understanding of the plateau's precipitation microphysical  
53 parameters through the study of raindrop spectral parameters and distribution characteristics in various  
54 regions.

55 Some studies have explored the spectral characteristics of raindrops over the Tibetan Plateau. Yu Jianyu  
56 et al. and Shu Lei et al. conducted analyses on the raindrop spectrum characteristics of various clouds in  
57 the Naqu and Yushu regions of the Qinghai–Tibet Plateau(Yu et al., 2020; Shu et al., 2021). Li Shanshan

58 et al. investigated raindrop spectral characteristics at different elevations on the eastern slope of the  
59 Qinghai–Tibet Plateau. They discovered that the average spectrum of raindrop number concentration at  
60 various elevations conforms to the Gamma function distribution. Moreover, light precipitation and heavy  
61 precipitation exhibit distinct raindrop spectral characteristics(Li et al., 2020). The aforementioned  
62 research was conducted in Naqu and Yushu areas in the Qinghai–Tibet Plateau, as well as the west  
63 Sichuan Plateau area. However, there is a limited number of studies on the spectral characteristics and  
64 distribution rules of cloud precipitation raindrops in various regions of the Tibetan Plateau. The analysis  
65 of raindrop spectrum characteristics in the Naqu region, as mentioned earlier, was conducted only during  
66 the summer months from June to August 2014. In this study, we used raindrop spectrum data from the  
67 Naqu region spanning 2017 to 2020, building upon and extending previous research. We analyzed the  
68 temporal variation of the raindrop spectrum in convective cloud precipitation across various regions and  
69 examined differences in raindrop spectra among these regions. We conducted a systematic analysis of  
70 raindrop spectrum data associated with moderate rain from four stations with varying altitudes,  
71 longitudes, and latitudes. We compared and analyzed the differences in drop spectrum characteristics  
72 among these four stations, which is of great significance for enhancing the scientific understanding of  
73 precipitation's influence in the plateau region.

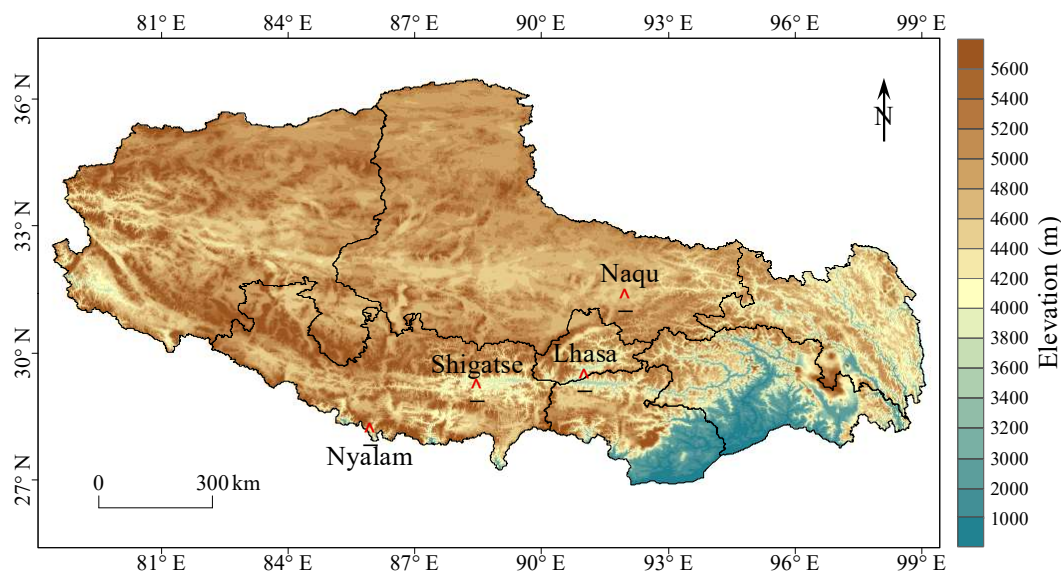
74 The objective of this study is to enhance the understanding of raindrop spectrum characteristics at various  
75 elevations of the Tibetan Plateau. The findings of this study will establish a foundation for  
76 comprehending precipitation characteristics and improving precipitation forecasts at diverse elevations  
77 of the Tibetan Plateau. This study is structured as follows: Data sources and research methods are  
78 described in Section 2. The analysis results are presented in Section 3 while the conclusion and discussion  
79 are provided in Section 4.

## 80 **2. Data and methods**

### 81 **2.1. Data collection**

82 The data obtained for this study consist of raindrop spectrum data from four meteorological stations (i.e.,  
83 Nyalam, Lhasa, Shigatse, and Naqu) in Tibet. Owing to its unique climate environment, snowfall occurs  
84 time to time from September to May. Data from June to August is selected to analyze the precipitation  
85 raindrop spectrum process in this study. The precipitation data selection criteria include a precipitation

86 process duration exceeding 20 minutes and a single precipitation process with rainfall greater than 5mm.  
 87 As the frequency of convective clouds in most areas of the Qinghai–Tibet Plateau exceeds 90%, all  
 88 collected samples are categorized as convective clouds in this paper. Table 1 displays the longitude,  
 89 latitude, altitude, and sample numbers of the four stations. Figure 1 illustrates the geographical  
 90 distribution of the four sites. The four stations cover a broad area of central Tibet from south to north,  
 91 making the results representative.



92  
 93 **Figure 1: Station distribution and the surrounding terrain**

94 **Table 1: Coordinates, elevation, sampling periods, and sample sizes of the four sites.**

Station	Longitude	Latitude	Elevation	Sampling period	Sample size
Nyalam	85.58° E	28.11° N	4519 m	2017–2019	11579
Lhasa	91.08° E	29.40° N	3653 m	2017–2018	8364
Shigatse	88.53° E	29.15° N	3910 m	2017–2018	14237
Naqu	92.04° E	31.29° N	4560 m	2017–2020	5630

95 **2.2. Quality Control and Quality Assurance (QA/QC)**

96 The Parsivel2 raindrop spectrometer features 32 particle size measurement channels and 32 particle  
 97 velocity measurement channels. The particle size measurement range is 0.062–24.5 mm, and the particle  
 98 velocity measurement range is 0.05–20.8 m s<sup>-1</sup>, with a sampling time of 60 s. In comparison to the  
 99 previous Parsivel raindrop spectrometer model, the Parsivel2 raindrop spectrometer utilizes infrared light  
 100 as its light source. This change reduces the interference of visible light, resulting in significant  
 101 advancements in the measurement of raindrop size and rainfall. Following the sampling principle of the

102 raindrop spectrometer, the instrument records the particle size and particle speed of all particles passing  
 103 through the sampling surface. To mitigate the influence of sand and dust particles, it is imperative to  
 104 control the quality of the fundamental data.

105 Atlas(Atlas et al., 1973) discovered a relationship between the terminal velocity of particles and the  
 106 particle diameter. In an ideal windless environment, the formula for the terminal velocity of particles is:

$$\begin{cases} v=0, & x < 0.03 \\ v = 4.323 \times (x - 0.03), & 0.03 \leq x \leq 0.6 \\ v = 9.65 - 10.3 \times e^{-0.6x}, & x > 0.6 \end{cases} \quad (1)$$

108 where  $x$  represents the particle diameter in mm, and  $v$  represents the terminal velocity of the particle in  
 109  $\text{m s}^{-1}$ . Equation (1) is applicable near the ground. For other altitudes, considering the known effect of  
 110 atmospheric air density on the terminal fall velocity, a correction factor for the fall velocity of raindrops,  
 111 accounting for air density, as given by Atlas et al. (1973) and Foote and du Toit et al. (1969),  $(\rho_0/\rho)^{0.4}$  is  
 112 multiplied on the right-hand side of Equation (1). Here,  $\rho$  is the air density at the observation altitude,  
 113 and  $\rho_0$  is the air density at sea level under standard atmospheric pressure.

114 Kruger and Krajewski(Kruger and Krajewski, 2002) proposed a method to mitigate the dispersion of  
 115 velocity over large samples, building on the study by Atlas. Initially, the terminal velocity was calculated  
 116 based on the particle diameter and final velocity formula, and subsequently, a threshold value was set for  
 117 elimination. The formula is expressed in Equation 2.

$$|v_{measured} - v_A| < 0.4v_A \quad (2)$$

118 where  $v_{measured}$  represents the final velocity measured by the raindrop spectrometer, and  $v_A$  is the final  
 119 velocity calculated using the final velocity formula. If the relative error falls within the specified  
 120 threshold range, the data will be retained.

122 Previous studies have highlighted that the distribution of raindrop spectra exhibit distinct characteristics  
 123 influenced by geographical environment and topography. Hence, utilizing the same calculation formula  
 124 across different areas for raindrop spectrum elimination is likely to introduce significant errors. Therefore,  
 125 we utilized historical data from a raindrop spectrum site to localize the parameters identified in the study  
 126 by Atlas and incorporates them into the formula for particle elimination. Simultaneously, due to  
 127 deformation occurring in raindrops during descent, the raindrop spectrum data undergoes distortion and  
 128 correction after quality control.

129 **2.3. Raindrop spectrum parameters**

130 The number density of the precipitation raindrop spectrum is defined as the total number of particles per  
131 unit volume(Shi et al., 2008).

$$132 \quad N(D) = \sum_{i=1}^{32} \sum_{j=1}^{32} \frac{n_{ij}}{A \cdot \Delta T \cdot V_j} \quad (3)$$

133 where N(D) is the number density parameter, in units of mm<sup>-1</sup> m<sup>-3</sup>; n<sub>ij</sub> represents the number of  
134 raindrops with the diameter of the i-th particle and the velocity of the j-th particle; A is the sampling  
135 base area of the raindrop spectrometer (5400 mm<sup>2</sup>); ΔT is the sampling time (60 s); V<sub>j</sub> is the velocity  
136 value of the sampled particle, in units of m s<sup>-1</sup>.

137 The average diameter is calculated as the sum of the diameters of all raindrops per unit volume divided  
138 by the total number of raindrops, and the formula is given by equation 4.

$$139 \quad D_l = \frac{\sum_{i=1}^{32} N(D_i) D_i}{\sum_{i=1}^{32} N(D_i)} \quad (4)$$

140 The weighted average diameter represents the average diameter of the weighted mass of all particles per  
141 unit volume relative to the total mass of particles, measured in mm. The formula is expressed in equation  
142 5.

$$143 \quad D_m = \frac{\sum_{i=1}^{32} N(D_i) D_i^4}{\sum_{i=1}^{32} N(D_i) D_i^3} \quad (5)$$

144 where D<sub>i</sub> represents the diameter of the i-th particle, and N(D<sub>i</sub>) represents the particle number density  
145 of the i-th particle diameter.

146 Precipitation intensity refers to precipitation per unit time (per hour), measured in mm h<sup>-1</sup>. The formula  
147 is given by equation 6.

$$148 \quad I = \frac{6\pi}{10^4} \sum_{i=1}^{32} D_i^3 V(D_i) N(D_i) \quad (6)$$

149 The radar reflectivity factor is the sum of the backscattering area of all particles per unit volume,  
150 measured in mm<sup>-6</sup> m<sup>-3</sup>. The formula is expressed in equation 7.

$$Z = \sum_{i=1}^{32} N(D_i) D_i^6 \quad (7)$$

151

152 The observed raindrop spectrum is discrete, and the double parameter index, namely Exponential  
 153 distribution, can be used to simulate the raindrop particle size distribution. The formula is given by  
 154 equation 8.

$$N(D) = N_0 \times \exp(-\lambda D) \quad (8)$$

155

156 where  $N_0$  is a number density parameter, measured in  $\text{mm}^{-1} \text{m}^{-3}$ .  $\lambda$  is a size parameter, measured in  $\text{mm}^{-1}$ .  
 157

158 However, this distribution pattern has some errors compared with actual observation data when  
 159 describing small and large raindrops. Therefore, Ulbrich and Atlas proposed a modified raindrop particle  
 160 size distribution pattern. They treated the raindrop spectrum distribution as a Gamma distribution to  
 161 correct the distribution pattern between small and large raindrops.

162 In this case, the raindrop particle size distribution follows the Gamma distribution with three  
 163 parameters(Carlton and David, 1984). The formula is given by equation 9.

$$N(D) = N_0 \times D^\mu \times \exp(-\lambda D) \quad (9)$$

164

165 where  $\mu$  is a dimensionless parameter referred to as the shape factor. When  $\mu$  is greater than 0, the curve  
 166 exhibits an upward curvature; when  $\mu$  is less than 0, the curve displays a downward curvature. When  
 167  $\mu=0$ , it corresponds to an Exponential distribution.

168 Zhang(Zhang et al., 2003) pointed out a binomial relationship between  $\mu$  and  $\lambda$  when studying the  $\mu$ - $\lambda$   
 169 relationship of precipitation in Florida:

$$\lambda = a\mu^2 + b\mu + c \quad (10)$$

170

171 Ulbrich(Ulbrich, 1983) pointed out in his study that the  $\mu$ - $\lambda$  relation under Gamma distribution can be  
 172 expressed as:

$$D_m = \frac{4+\mu}{\lambda} \quad (11)$$

173

174 Equation (11) shows that there is a relationship between the ratio of  $\mu$  and  $\lambda$  and the weighted average  
 175 diameter of mass. The Gamma distribution fit is typically applied to the observed raindrops distribution  
 176  $N(D)$  using the least squares or order moments method. In this study, the least square method is employed  
 177 to fit the Exponential and Gamma distributions.

178 **3. Result and discussion**

179 The average altitude of the Qinghai–Tibet Plateau is over 4000 m, and the terrain is complex and  
 180 changeable, resulting in varying microphysical characteristics of the raindrop spectrum. Therefore,  
 181 considering the unique conditions of the Qinghai–Tibet Plateau, the rain intensity calculated based on  
 182 the raindrop spectrum was categorized into five grades for calculation and analysis, as presented in Table  
 183 2. The samples from the four stations in the range of 0.5–5 mm·h<sup>-1</sup> were the largest, and the obtained  
 184 standard deviation values were all very small. This indicates a high consistency in rain intensity  
 185 distribution under weak rain intensity. In the interval of precipitation intensity greater than 20 mm h<sup>-1</sup>,  
 186 only two stations have samples, and one of the stations exhibits a large standard deviation. This reflects  
 187 a significant inversion error in raindrop spectrum for Nyalam during short–duration heavy precipitation.

188 **Table 2: Descriptive statistics of rainfall intensity at the four stations.**

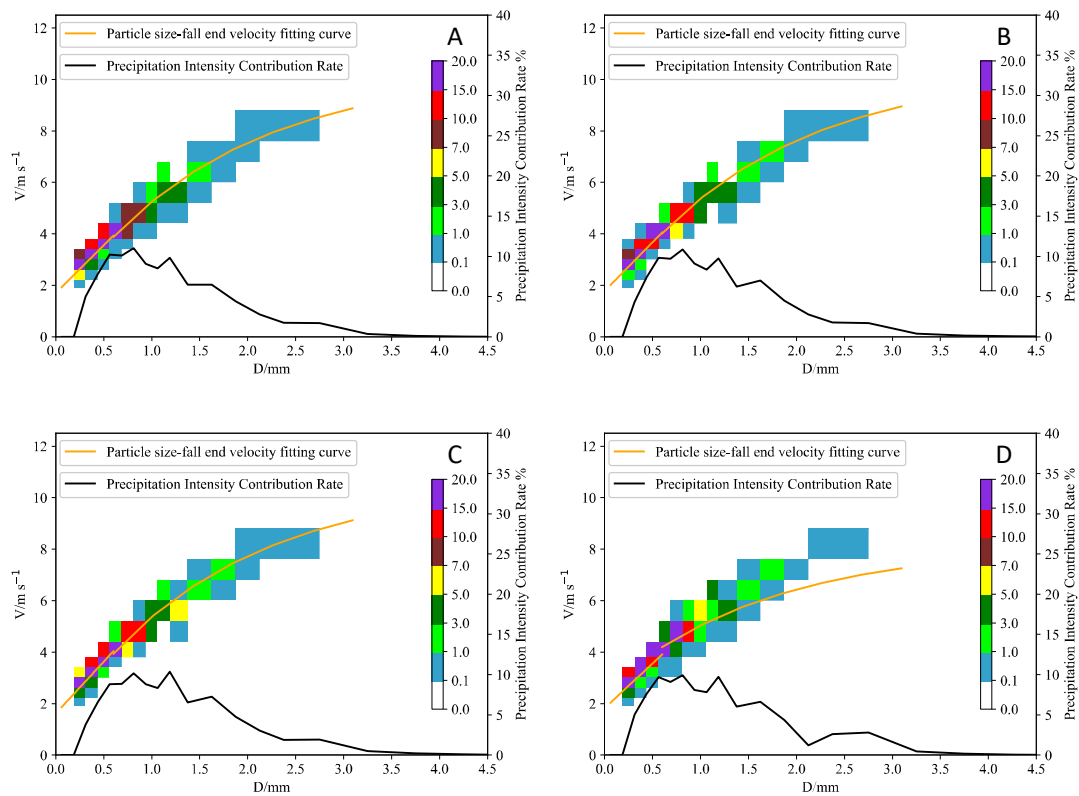
	Range (mm·h <sup>-1</sup> )	Sample Size	Mean (mm·h <sup>-1</sup> )	Standard Deviation	Precipitation (mm)
Nyalam	0.5–5	4047	2.16	1.21	146
	5–10	1358	7.38	1.28	166.6
	10–15	900	12.14	1.32	182.1
	15–20	656	17.69	1.37	193.4
	>20	960	30.63	7.99	490
Lhasa	0.5–5	3245	1.8	0.94	97.4
	5–10	180	5.87	0.77	17.6
	10–15	50	12.1	0	12.1
	15–20	0	0	0	0
	>20	0	0	0	0
Shigatse	0.5–5	7094	1.78	1.06	210.7
	5–10	584	6.37	1.11	62.02
	10–15	60	10.01	0	10.01
	15–20	0	0	0	0
	>20	0	0	0	0
Naqu	0.5–5	2389	3.27	1.5	130.1



5–10	675	7.76	1.1	87.3
10–15	479	13.73	1.21	109.6
15–20	372	19.65	1.4	121.8
>20	120	21.6	1.5	43.2

189 **3.1. Precipitation particle size, speed and rainfall intensity contribution rate distribution**

190 Figure 2 represent the mean precipitation values across the four stations. The canvas is divided into  
191 several rectangular areas defined by the coordinates of the horizontal and left axes, and the color code is  
192 applied to them. Each rectangular area represents a specific particle diameter and velocity. Figure 2  
193 reveals that the fitting curves of particle diameter distribution and terminal velocity at the four stations  
194 are approximately identical, and the terminal velocity increases with the particle diameter. Regarding  
195 particle number density, it is concentrated in the area with particle size less than 1 mm, and it decreases  
196 with the increase of diameter. Concerning the contribution rate of precipitation intensity, the four stations  
197 exhibit a multi-peak distribution, with peak diameters at 0.812 mm and 1.375 mm. In comparison with  
198 the precipitation process of convective clouds at low-altitude stations, the particle size spectrum width  
199 at the four stations on the Tibetan Plateau in this analysis was notably reduced, and the particle number  
200 density at the four stations with particle sizes greater than 3 mm was very low.



201

202 **Figure 2: The average spectrum of precipitation particle size, velocity, and contribution rate distribution of**  
 203 **precipitation intensity. The color bar represents the number density in units per m<sup>3</sup>. (A. Nyalam, B. Lhasa,**  
 204 **C. Shigatse, and D. Naqu).**

205 Figure 3 displays the fitting relationship between the particle size of the raindrop spectrum and the falling  
 206 speed at the four stations in Tibet. For particle sizes less than 1.5 mm, the particle size at the four stations  
 207 essentially aligns with the final falling speed. For particle sizes greater than 1.5 mm, the speed is largest  
 208 for Nyalam, followed by Naqu, and Lhasa has the smallest speed. However, under the same size, the  
 209 final velocities of particles at the four stations are greater than those in Guizhou, exceeding 2 m/s. This  
 210 may be attributed to the higher altitude of the four stations, which are over 3000 m above sea level. This  
 211 indicates that the high altitude of Tibet, due to thin air and low air pressure, results in decreased fall speed  
 212 of larger particles of the same size. However, particles at lower altitudes (Shigatse and Lhasa) exhibited  
 213 slightly Lower speeds than those at higher altitudes (Nyalam and Naqu). The fitting formulas for the  $v$ - $D$   
 214 relationships at the four sites (Nyalam, Lhasa, Shigatse, and Naqu) are given by Equations 12, 13, 14,  
 215 and 15, respectively. Considering the effect of air density on the fall velocity of raindrops as per Atlas et  
 216 al. (1973), the correction factor  $(\rho_0/\rho)^{0.4}$  is multiplied to Equations 12, 13, 14, and 15, resulting in the  
 217 fitting relationship curves between the particle size of the raindrop spectrum and the falling speed at the

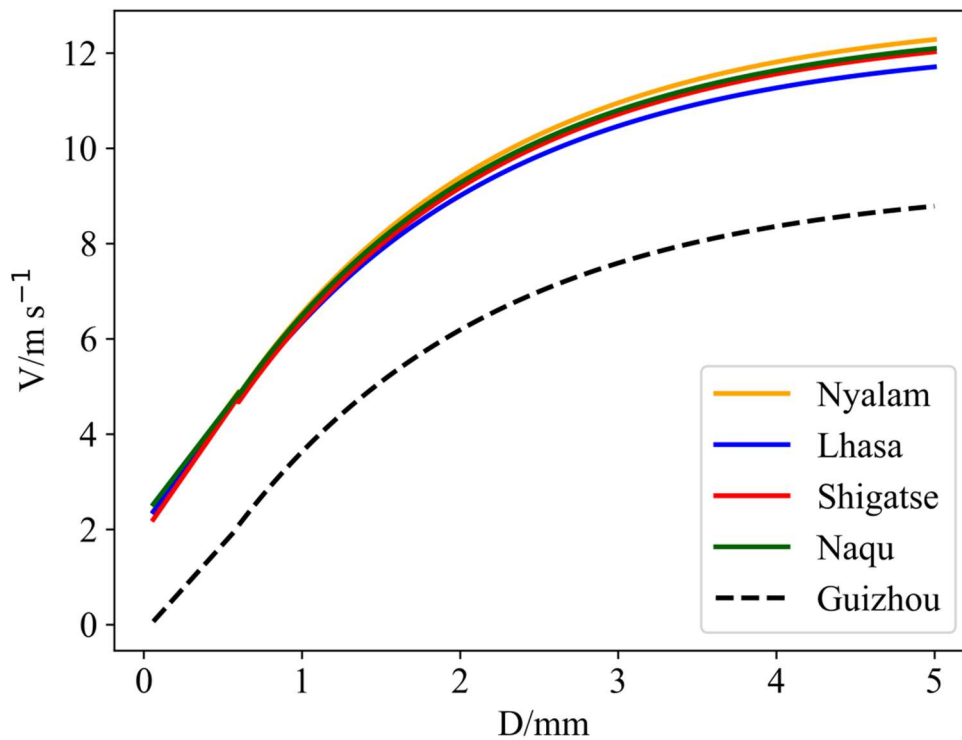
218 four stations in Tibet shown in Figure 3. The correction factor for fall velocity considering air density is  
 219 shown in Table 3.

$$\begin{cases} v=0, & x < 0.03 \\ v = 3.720 \times (x+0.456), & 0.03 \leq x \leq 0.6 \\ v = 10.325 - 9.252 \times e^{-0.6x}, & x > 0.6 \end{cases} \quad (12)$$

$$\begin{cases} v=0, & x < 0.03 \\ v = 3.796 \times (x+0.468), & 0.03 \leq x \leq 0.6 \\ v = 10.375 - 9.118 \times e^{-0.6x}, & x > 0.6 \end{cases} \quad (13)$$

$$\begin{cases} v=0, & x < 0.03 \\ v = 4.035 \times (x+0.401), & 0.03 \leq x \leq 0.6 \\ v = 10.614 - 9.568 \times e^{-0.6x}, & x > 0.6 \end{cases} \quad (14)$$

$$\begin{cases} v=0, & x < 0.03 \\ v = 3.474 \times (x+0.524), & 0.03 \leq x \leq 0.6 \\ v = 10.162 - 9.018 \times e^{-0.6x}, & x > 0.6 \end{cases} \quad (15)$$



224  
 225 **Figure 3: The relationship between particle size and speed at four stations.**

226 **Table 5: The correction factor for fall velocity considering air density**

Correction factor $((\rho_0/\rho)^{0.4})$				
Nyalam	Lhasa	Shigatse	Naqu	

1.240                      1.179                      1.185                      1.240

227

228 The proportion of particle number density in raindrop spectrum and the contribution rate of precipitation  
 229 are shown in Table 4 and Table 5, respectively.

230 **Table 4: Percentage of particle number density.**

	Particle diameter (mm)		
	0–1 mm	1–2 mm	2–3 mm
Nyalam	93.60	6.15	0.25
Lhasa	92.41	7.24	0.35
Shigatse	91.45	8.06	0.49
Naqu	91.89	7.52	0.59

231 **Table 5: Percentage of precipitation contribution rate.**

	Particle diameter (mm)		
	0–1 mm	1–2 mm	2–3 mm
Nyalam	55.63	37.32	7.05
Lhasa	54.60	38.16	7.24
Shigatse	51.12	40.49	8.39
Naqu	54.06	37.81	8.13

232 It can be observed from Table 3 that the number of precipitation particles with a distribution of 0–1 mm  
 233 constitutes the largest proportion, exceeding 91%, while the proportion of particles with a distribution of  
 234 more than 3 mm is comparatively smaller, being less than 0.6%. The proportion of precipitation intensity  
 235 below 1 mm constitutes over 51%, with other particles comprising less than 49%. The results indicate  
 236 that the contribution of precipitation intensity on the Tibetan Plateau is primarily concentrated in small  
 237 particles with a diameter less than 1 mm.

238 In contrast to the convective cloud precipitation in Zheng’an, Guizhou analyzed by Wang(Wang et al.,  
 239 2020), where convective cloud particles less than 1 mm account for 64.4%, the contribution rate to  
 240 precipitation is only 17%; Additionally, it significantly differs from the rainstorm in Hainan analyzed by  
 241 Mao(Mao et al., 2020). Despite the proportion of less than 1mm being 82.7%, the contribution rate is  
 242 only 18.2%, and the rainstorm particle size spectrum in Hainan is remarkably wide. It is evident that the  
 243 precipitation characteristics of convective clouds on the Qinghai–Tibet Plateau exhibit a particularity,

244 wherein the diameter of precipitation particles is generally small, and the precipitation of small-diameter  
245 particles constitutes a substantial proportion of the total precipitation.

### 246 **3.2. Microphysical characteristic parameters of precipitation**

247 The calculation of microphysical parameters based on raindrop spectra is divided into five levels  
248 according to different rainfall intensities. The average diameter ( $D_m$ ), mean volume diameter ( $D_v$ ), mode  
249 diameter ( $D_d$ ), dominant diameter ( $D_p$ ), and median diameter ( $D_{nd}$ ) were calculated for four stations.  
250 Comprehensive analysis based on the characteristic parameters in Tables 6, 7, 8, and 9 shows that, under  
251 the same rainfall intensity level,  $D_m$  decreases with increasing altitude. The  $D_m$  at the higher-altitude  
252 Naqu and Nyalam stations is smaller than at the lower-altitude Lhasa and Shigatse stations. Under the  
253 same rainfall intensity level,  $D_v$  increases with altitude, with the smallest value at the low-altitude Lhasa  
254 station and the largest at the high-altitude Naqu station. When the rainfall intensity is less than  $\text{mm}\cdot\text{h}^{-1}$ ,  
255  $D_d$  increases with altitude (except for the Nyalam station), with the largest value at the Naqu station and  
256 the smallest at the Lhasa station, with the Shigatse station in between. When the rainfall intensity is  
257 greater than  $10\text{mm}\cdot\text{h}^{-1}$ ,  $D_d$  decreases with altitude, with the largest value at the Lhasa station and the  
258 smallest at the Nyalam station, with the Shigatse and Naqu stations in between. When the rainfall  
259 intensity is less than  $10\text{mm}\cdot\text{h}^{-1}$ ,  $D_p$  does not show a significant difference with altitude under the same  
260 rainfall intensity level. However, when the rainfall intensity is greater than  $10\text{mm}\cdot\text{h}^{-1}$ ,  $D_p$  increases  
261 with altitude under the same rainfall intensity level (except for the Nyalam station). For the lower-altitude  
262 Lhasa and Shigatse stations, there is no significant difference in parameters under the same rainfall  
263 intensity. In contrast, for the higher-altitude Naqu and Nyalam stations, there are relatively obvious  
264 differences in parameters under the same rainfall intensity, with the Nyalam station's values being  
265 significantly smaller than those of the Naqu station. The reason for the smaller values at the Nyalam  
266 station compared to the nearby altitude Naqu station might be due to its unique geographical conditions.  
267 The above analysis indicates a strong correlation between altitude and these microphysical parameters.  
268  $D_m$  shows a negative correlation with altitude under the same rainfall intensity, while  $D_v$  shows a  
269 positive correlation with altitude. For  $D_d$  and  $D_p$ , using  $10\text{mm}\cdot\text{h}^{-1}$  as the dividing line, there are  
270 different correlations with altitude under the same rainfall intensity level. Additionally, when the altitude  
271 is below 4000 m, there is no significant difference in characteristic diameters under the same rainfall  
272 intensity. Conversely, when the altitude is above 4000 m, the differences in characteristic diameters

273 become more pronounced.

274 **Table 6: Microphysical parameters of the Lhasa station.**

	Range (mm·h <sup>-1</sup> )	Dm	Dv	Dd	Dp	Dnd
Lhasa	0.5-5	0.636	1.744	0.470	1.277	1.105
	5-10	0.809	2.058	0.671	1.869	1.628
	10-15	0.981	2.231	1.096	2.229	2.058
	15-20	1.008	2.288	1.069	2.256	2.095
	>20	1.063	2.421	1.331	2.744	2.580

275 **Table 7: Microphysical parameters of the Shigatse station.**

	Range (mm·h <sup>-1</sup> )	Dm	Dv	Dd	Dp	Dnd
Shigatse	0.5-5	0.641	1.748	0.473	1.291	1.126
	5-10	0.815	2.044	0.685	1.901	1.639
	10-15	0.970	2.216	1.041	2.293	2.088
	15-20	1.000	2.298	1.277	2.612	2.292
	>20	1.045	2.409	1.200	2.833	2.566

276 **Table 8: Microphysical parameters of the Nyalam station.**

	Range (mm·h <sup>-1</sup> )	Dm	Dv	Dd	Dp	Dnd
Nyalam	0.5-5	0.593	1.764	0.415	1.282	1.088
	5-10	0.725	2.064	0.498	1.865	1.574
	10-15	0.823	2.163	0.601	2.062	1.720
	15-20	0.905	2.217	0.846	2.351	2.022
	>20	0	0	0	0	0

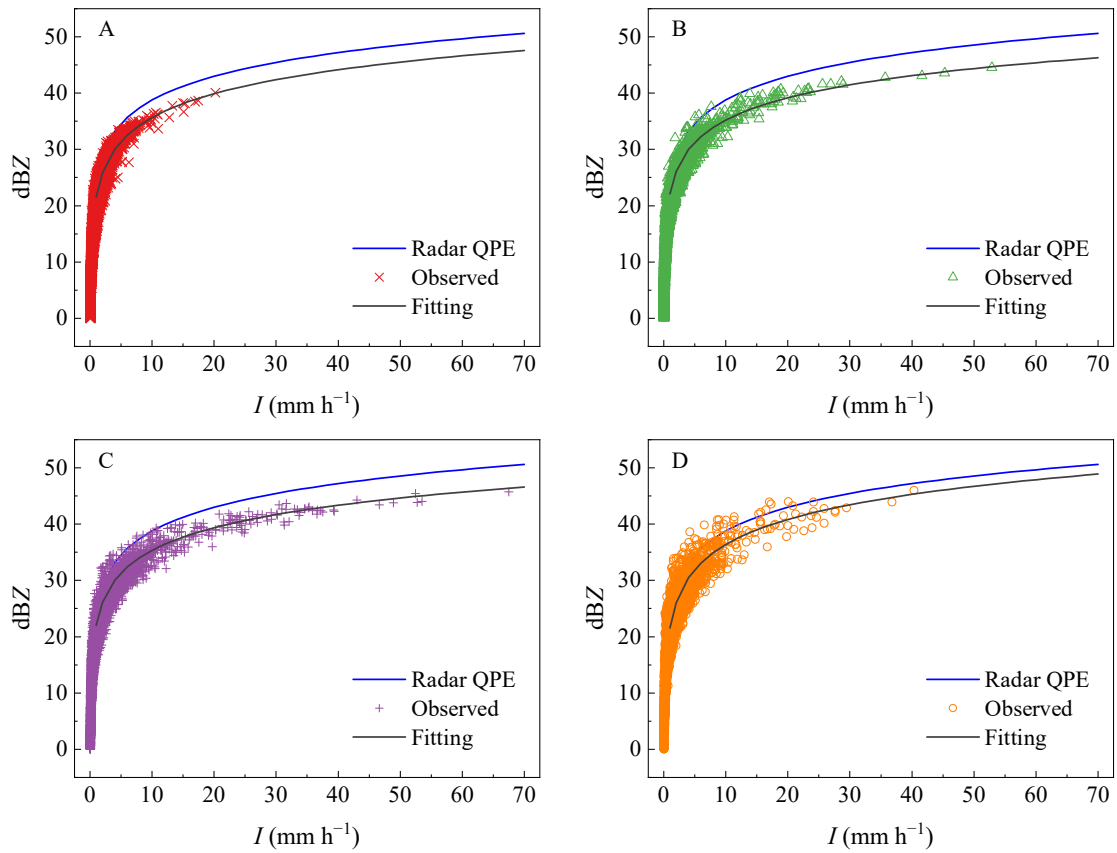
277 **Table 9: Microphysical parameters of the Naqu station.**

	Range (mm·h <sup>-1</sup> )	Dm	Dv	Dd	Dp	Dnd
Naqu	0.5-5	0.621	1.758	0.491	1.268	1.110

5-10	0.808	2.071	0.777	1.730	2.022
10-15	0.922	2.250	0.947	2.434	2.205
15-20	0.970	2.313	1.005	2.595	2.291
>20	1.043	2.479	1.166	3.004	2.673

278 **3.3. Z-I relation distribution**

279 Utilizing Formulae (6) and (7), the radar reflectivity (Z) and precipitation intensity (I) are calculated  
 280 independently, and the data undergo fitting. The results are depicted in Figure 4.



281  
 282 **Figure 4: The Z-I relationships at four stations. (A. Nyalam, B. Lhasa, C. Shigatse, and D. Naqu)**

283 Figure 4 reveals that the suggested reference relation  $Z=300 \times I^{1.4}$  inaccurately predicts precipitation,  
 284 leading to an underestimation of precipitation intensity under identical radar reflectivity. With identical  
 285 radar reflectance, the precipitation intensity is highest in Lhasa, followed by Shigatse, while the smallest  
 286 precipitation intensity was observed in Naqu.

287 Table 7 shows the results of fitted Z-I relationships. Analyzing the altitude based differences in the Z-I  
 288 relationship, the a and b coefficients are similar for the station at 3653 m (Lhasa) and the station at 3910  
 289 m (Shigatse), while a and b for the station at 4519 m (Nyalam) and the station at 4560 m (Naqu) are

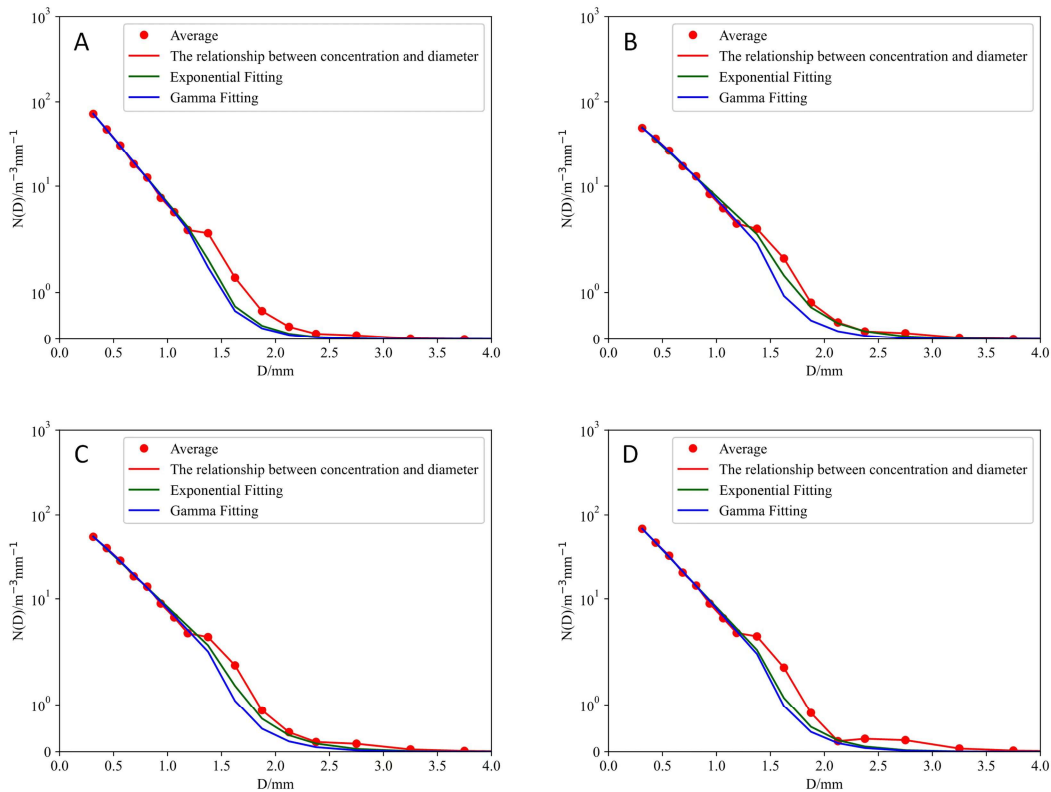
290 close. This observation indicates that the fitting parameter  $a$  is notably smaller, and the fitting parameter  
 291  $b$  is larger for stations at higher altitudes.

292 **Table 10: Z-I relationship fitting results.**

	$Z = aI^b$		
	Fitting	$a$	$b$
Nyalam	$Z=143.01 \times I^{1.41}$	143.01	1.41
Lhasa	$Z=162.56 \times I^{1.31}$	162.56	1.31
Shigatse	$Z=160.21 \times I^{1.33}$	160.21	1.33
Naqu	$Z=143.81 \times I^{1.48}$	143.81	1.48

293 **3.4. Precipitation particle distribution fitting**

294 According to Formulas (8) and (9), the least squares method is applied to fit the Exponential and Gamma  
 295 distributions of the mean raindrop spectrum of precipitation at the four stations. The results are presented  
 296 in Figure 5 and Table 7.



297  
 298 **Figure 5: Exponential and Gamma intriutions for precipitation (A. Nyalam, B. Lhasa, C. Shigatse, and D.**  
 299 **Naqu).**

300 As indicated in Table 8,  $\mu$  decreases with increasing altitude in the Gamma distribution. A smaller  $\mu$



301 corresponds to a wider raindrop spectrum, signifying that the diameter of raindrops increases with  
302 altitude. The raindrop diameter at higher altitudes is larger, corresponding to the precipitation  
303 microphysical characteristics calculated in Table 6. Conversely, the fitting results of the Exponential  
304 distribution show that  $N_0$  and  $\lambda$  exhibit a clear increasing trend with height. In Figure 5, the abscissa  
305 represents particle diameter, and the ordinate represents particle number density. The curve trends at the  
306 four stations are relatively consistent. For Nyalam station, the Exponential distribution is given by  
307  $N(D)=218.78 \times e^{-3.53D}$ , and the Gamma distribution is  $N(D)=282.14 \times D^{0.15} \times e^{-3.82D}$ . For Lhasa  
308 station, the Exponential distribution is  $N(D)=118.70 \times e^{-2.75D}$ , and the Gamma distribution is  
309  $N(D)=250.40 \times D^{0.43} \times e^{-3.56D}$ . For Shigatse station, the Exponential distribution is  
310  $N(D)=130.35 \times e^{-2.79D}$ , and the Gamma distribution is  $N(D)=216.08 \times D^{0.29} \times e^{-3.35D}$ . Finally, for  
311 Naqu station, the Exponential distribution is  $N(D)=177.22 \times e^{-3.10D}$ , and the Gamma distribution is  
312  $N(D)=238.95 \times D^{0.17} \times e^{-3.44D}$ . In the Gamma distribution, two parameters,  $\mu$  and  $\lambda$ , represent the curve  
313 shape factor and particle scale parameters, respectively, as shown in Equation (9). According to Equation  
314 (10), the two parameters  $\mu$  and  $\lambda$  for the four stations are fitted with an analytical binomial relationship,  
315 and the coefficients are presented in Table 9.

316 **Table 11: Gamma fitting and Exponential fitting results.**

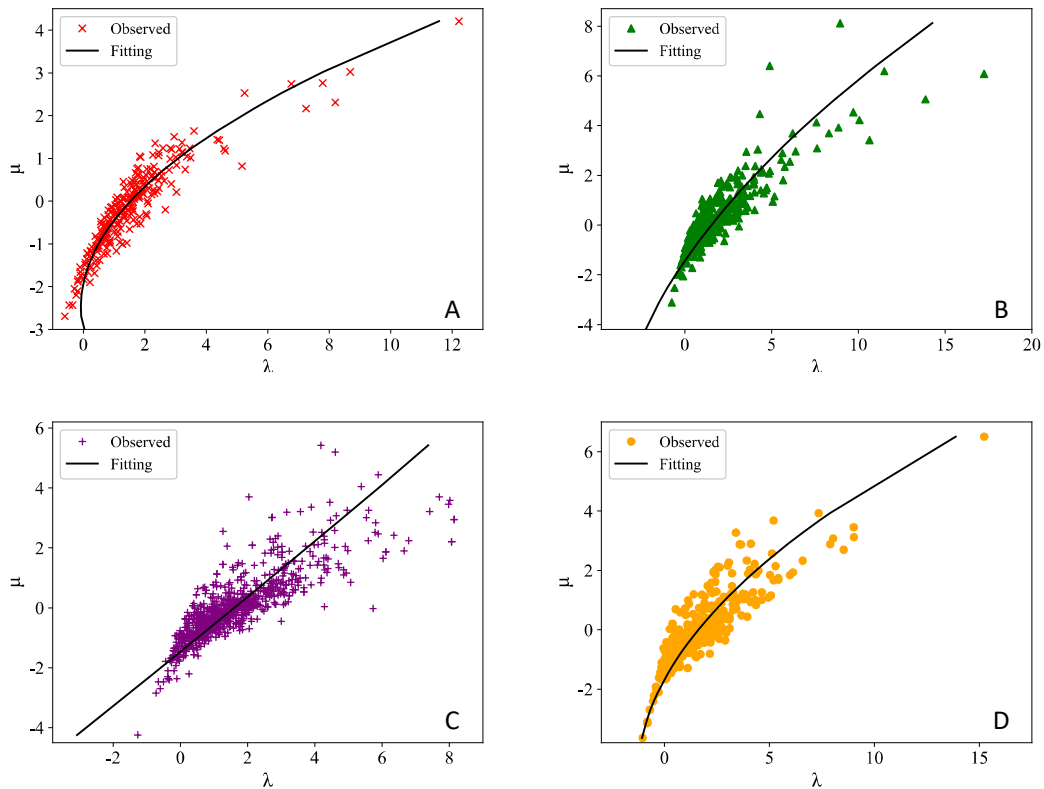
	Gamma			Exponential	
	$N_0$	$\mu$	$\lambda$	$N_0$	$\lambda$
Nyalam	284.90	0.15	3.83	218.93	3.53
Lhasa	253.26	0.44	3.59	118.81	2.75
Shigatse	217.69	0.30	3.35	130.45	2.79
Naqu	240.91	0.18	3.45	177.34	3.10

317 **Table 12:  $\mu$  and  $\lambda$  binomial parameters**

	$\lambda = a\mu^2 + b\mu + c$		
	$a$	$b$	$c$
Nyalam	0.2816	1.2798	1.5074
Lhasa	0.1717	1.0589	1.3983
Shigatse	0.0221	1.1215	1.6002
Naqu	0.0155	1.2141	1.7599

318 It can be observed from Figure 6 that, although the four curves bend towards the lambda axis, the degree  
319 of bending varies. The curves for Shigatse exhibit nearly straight curves, whereas the curves for Nyalam  
320 and Naqu are more pronounced in their curvature towards the lambda axis. The  $\mu$ - $\lambda$  relationship varies  
321 among the four stations, and this variation is associated with the mass-weighted diameter. Eq. (11)

322 indicates that when  $\lambda$  remains constant, a higher  $\mu$  value corresponds to a greater mass-weighted average  
323 diameter.



324  
325 **Figure 6:  $\mu$ - $\lambda$  relationship (A. Nyalam, B. Lhasa, C. Shigatse, D. Naqu).**

#### 326 4. Conclusions

327 In this study, we conducted a statistical analysis of raindrop spectrum data above light and moderate rain  
328 at four sites in Tibet, considering different heights, latitudes, and longitudes. The analysis includes  
329 precipitation particle size distribution, particle landing speed, precipitation particle number density, and  
330 rainfall intensity at the end. Additionally, the relationship between Z-I distribution and rainfall rate,  
331 precipitation particle distribution fitting, and analysis of Gamma distribution  $\mu$ - $\lambda$  parameters for the  
332 precipitation raindrop spectrum characteristics at the four stations are examined. A comparison is made  
333 between the data from the four stations on the Qinghai-Tibet Plateau and some non-plateau areas.  
334 Simultaneously, the analysis of raindrop spectrum data at the Naqu station reveals certain similarities  
335 with previous studies (indicating convective cloud as the primary precipitation at Naqu station). However,  
336 some differences are noted, such as the mean spectral width of convective precipitation at the Naqu  
337 station being relatively narrow.

338 The relationship between precipitation particle size and particle landing velocity at the four stations  
339 indicates that the terminal velocity of the four stations essentially coincided when the particle size was  
340 less than 1.5 mm. For particle sizes greater than 1.5 mm, the terminal velocity of particles at the four  
341 stations is faster at high altitudes than at medium and low altitudes. At the four stations, the proportion  
342 of precipitation raindrop spectral particle size less than 1 mm exceeded 91%, and the contribution rate of  
343 precipitation was more than 51%. The characteristics of convective cloud precipitation over the Tibetan  
344 Plateau exhibit peculiarities that differ from the raindrop spectrum characteristics in the low–altitude  
345 areas of the mainland.

346 The six microphysical characteristics at the four stations have different correlation relationships with  
347 altitude under different rainfall intensities.  $D_m$  exhibits a negative correlation with altitude at the same  
348 rainfall intensity; in contrast,  $D_v$  shows a positive correlation with altitude. For microphysical parameters  
349 such as  $D_d$  and  $D_p$ , a rainfall intensity of  $10 \text{ mm} \cdot \text{h}^{-1}$  serves as the boundary line, and they have different  
350 correlation relationships with altitude under the same rainfall intensity level. Regarding the fitted  $Z-I$   
351 relationship, the fitting parameter  $a$  at the high–altitude station is significantly smaller, while the fitting  
352 parameter  $b$  is larger. The particle spectrum of high–altitude stations is broader, with a larger equivalent  
353 diameter, and the reflectivity of high–altitude stations is significantly higher than that of low–altitude  
354 stations.

355 The concentration of small raindrops (less than 1 mm) in the raindrop spectrum of high–altitude stations  
356 on the Tibetan Plateau was higher. Both the Exponential distribution and the Gamma distribution exhibit  
357 good fitting effects for low–altitude stations. Overall, the Exponential fit performed better. In the  
358 relationship between the  $\mu$  and  $\lambda$  of the two parameters in the Gamma distribution, the larger the  $\mu$ , the  
359 larger the weighted average diameter of the mass when the  $\lambda$  remains constant. In other words, the greater  
360 the  $\mu$ , the greater the precipitation intensity when  $\lambda$  remains unchanged.

#### 361 **Data Availability Statement**

362 The data used to support the findings of this study are available from the corresponding author upon  
363 request.

364 **Author Contributions**

365 Conceptualization, F.W. and G.C.; methodology, F.W. and Q.W.; software, Y.H. and Q.W.; writing—  
366 review and editing, F.W., Y.H. and Y.C.; resources, T.Z. and J.L.; supervision, T.Z. and G.C. All authors  
367 have read and agreed to the published version of the manuscript.

368 **Competing interests**

369 The contact author has declared that none of the authors has any competing interests.

370 **Disclaimer**

371 Publisher’s note: Copernicus Publications remains neutral with regard to jurisdictional claims made in  
372 the text, published maps, institutional affiliations, or any other geographical representation in this paper.  
373 While Copernicus Publications makes every effort to include appropriate place names, the final  
374 responsibility lies with the authors.

375 **Acknowledgements**

376 We thank the Tibet Meteorological Bureau for the raindrop spectrum data, and the students and teachers  
377 of Chengdu University of Information Technology for their help.

378 **Financial support**

379 This research was funded by the Open Fund project for Key Laboratory of Land Surface Process and  
380 Climate Change in Cold and Arid Regions, Chinese Academy of Sciences (LPCC2020009), and the  
381 Natural Science Foundation of Sichuan Province (2022NSFSC0208) and National Natural Science  
382 Foundation of China (42075001).

383 **References**

384 Atlas, D., Srivastava, R. C., and Sekhon, R. S.: Doppler characteristics of precipitation at vertical  
385 incidence, *Rev. Geophys.*, 1973, 11, 1-35, doi:10.1029/RG011i001p00001, 1973.

386 Battaglia, A., Rustemeier, E., Tokay, A., Blahak, U., and Simmer, C: PARSIVEL snow observations: A

387 critical assessment, *J. Atmos. Ocean. Tech*, 27, 333-344, doi: 10.1175/2009JTECHA1332.1, 2010.

388 Chang, Y., and Guo, X. L.: Characteristics of convective cloud and precipitation during summer time at  
389 Nagqu over Tibetan Plateau, *Sci. Bull*, 61, 1706–1720, doi:10.1360/N972015-01292, 2016.

390 Carlton, W. U., and David, A.: Assessment of the contribution of differential polarization to improved  
391 rainfall measurements, *Radio Science*, 19, 49-57, doi:10.1029/RS019i001p00049, 1984.

392 Jiang, J. X., and Fan, M. Z.: Convective clouds and mesoscale convective systems over the Tibetan  
393 Plateau in summer, *Chin. J. Atmos. Sci*, 26, 263-270, doi:10.3878/j.issn.1006-9895.2002.02.12, 2002.

394 Kruger, A., and Krajewski, W. F.: Two-Dimensional Video Disdrometer: A Description, *J. Atmos. Ocean.*  
395 *Tech*, 19, 602-617, doi:10.1175/1520-0426(2002)019<0602:TDVDAD>2.0.CO, 2002.

396 Li, D., Bai, A. J., Xue, Y. J., and Wang, P.: Comparative analysis on characteristics of summer convective  
397 precipitation over Ti-betan Plateau and Sichuan Basin, *Meteor. Mon.*, 40, 280-289, doi:  
398 10.7519/j.issn.1000-0526.2014.03.003, 2014.

399 Li, L. G., and De, L. G. E.: Analyses of microphysical features for spring precipitation cloud layers in  
400 east of Qinghai, *Plateau Meteorology*, 20, 191-196, doi:10.3321/j.issn:1000-0534.2001.02.013, 2001.

401 Liu, L. P., Zheng, J. F., Ruan, Z., Cui, Z. H., Hu, Z. Q., Wu, S. H., et al.: The preliminary analyses of the  
402 cloud properties over the Tibetan Plateau from the field experiments in clouds precipitation with the  
403 various radars, *Acta. Meteor. Sin*, 73, 635-647, doi:10.11676/qxxb2015.041, 2015.

404 Li, S. S., Wang, X. F., Wan, R., and Li, G. P.: The Characteristics of Raindrop Spectrum in Different  
405 Altitude Region on the Eastern Slope of Qinghai-Xizang Plateau, *Plateau Meteorology*, 39, 899-911,  
406 doi:10.7522/j.issn.1000-0534.2019.00086, 2020.

407 Marshall, J. S., and Palmer, W. M.: The Distribution of Raindrops with Size, *J. Meteor*, 5, 165-166,  
408 doi: 10.1175/1520-0469(1948)005<0165:TDORWS>2.0.CO;1948

409 Mao, Z. Y., Huang, G. R., Huang, Y. B., Li, G. W., and Xing, F. H.: Characteristics Analysis of Raindrop  
410 Size Distribution during Hainan Autumn-Rainstorm Process, *Natural Science Journal of Hainan*  
411 *University*, 38, 59-66, doi:10.15886/j.cnki.hdxzbkb.2020.0009, 2020.

412 Ruan, Z., Jin, L., Ge, R. S., Li, F., and Wu, J.: The C-band FMCW pointing weather radar system and its  
413 observation experiment, *Acta. Meteor. Sin*, 3, 577-592, doi:10.11676/qxxb2015.039, 2015.

414 Shu, L., Li, M. S., Hua, S., Suo, L. J. C., Lv, Z., Fu, W., et al.: Statistical Characteristics of Raindrop Size  
415 Distribution and Microphysical Structure of Cloud in Yushu Region of Qinghai Tibet Plateau, *Advances*  
416 *in Meteorological Science and Technology*, 11, 113-121+134, doi:10.3969/j.issn.2095-1973.2021.04.016,

417 2021.

418 Shi, J. S., Zhang, W., Chen, T. Y., Bi, J. R., and He, M.: Raindrop-size distribution characteristics of the  
419 northern face of Qilian Mountains in the summer of 2006, *J. Lanzhou University(Natural Sciences)*, 44,  
420 55-61, doi: 10.3321/j.issn:0455-2059.2008.04.011, 2008.

421 Ulbrich, C. W.: Natural Variations in the Analytical Form of the Raindrop Size Distribution, *J. Climate*.  
422 *Appl. Meteor*, 22, 1764-1775, doi:10.1175/1520-0450(1983)022<1764:NVITAF>2.0.CO;2, 1983.

423 Wang, F. Z., Wang, Q. S., He, S., Gu, X. P., and Yu, F.: Analysis of Summer Raindrop Spectrum  
424 Characteristics of Zheng'an in Guizhou, *J. Chengdu University. Inf Technology*, 35, 689-696,  
425 doi:10.16836/j.cnki.jcuit.2020.06.016, 2020.

426 Xu, X. D., and Chen, L. S.: Advances of study on Tibetan Plateau experiment of atmospheric sciences,  
427 *J. Appl. Meteor. Sci*, 17, 756-772, doi:10.3969/j.issn.1001-7313.2006.06.013, 2006

428 Xiong, J. N., Li, W., Liu, Z. Q., Cheng, W. M., Fan, C. K., and Zhang, H.: Monitoring and analysis of  
429 historical drought in southeast Tibet based on multi--source data, *Arid Land Geography*, 42, 735-744,  
430 doi:10.12118/j.issn.1000—6060.2019.04.04, 2019.

431 Yu, J. Y., Li, M. S., and Yin, S. C.: Analysis of Cloud Precipitation Microscopic Characteristic Raindrop  
432 Spectrum in Nagqu Area of Qinghai-Tibet Plateau, *J. Chengdu University. Inf Technology*, 35, 188-194,  
433 doi:10.16836/j.cnki.jcuit.2020.02.010, 2020.

434 Zhang, N. J., Xiao, T. G., and Jia, L.: Spatial and Temporal Characteristics of Precipitation in the Tibet  
435 Plateau from 1979 to 2016, *J. Arid. Meteorology*, 36, 373-382, doi:10.11755/j.issn.1006-7639(2018)-03-  
436 0373, 2018.

437 Zhang, G., Vivekanandan, J., Brandes, E. A., Meneghini, R., and Kozu, T.: The Shape-Slope Relation in  
438 Observed Gamma Raindrop Size Distributions: Statistical Error or Useful Information?, *J. Atmos. Ocean*.  
439 *Tech*, 20, 1106-1119, doi:10.1175/1520-0426(2003)020<1106:TSRIOG>2.0.CO;2, 2003.